Chalcogenide Letters

Tech Science Press

http://doi.org/10.32604/cl.2026.081101

ARTICLE

Photoelectric Properties of Amorphous Selenium Thin Films Deposited by Thermal Evaporation

Zhadyra Toreniyaz[1], Guzal Ismailova[1], Oleg Prikhodko[1], Zhasulan Nakysbekov[1], Tilek Kuanyshbekov[2], Nurkadam Tolep[1], Dmitry Terekhov[3] and Zhandos Tolepov[1,*]

[1]Department of Physics and Technology, Al-Farabi Kazakh National University, Al-Farabi Avenue, 71, Almaty, Kazakhstan
[2]Kaz Graphene Limited Liability Partnership, Western str., 63, Ust-Kamenogorsk, Kazakhstan
[3]National Research University of Electronic Technology, Shokina str., 1, Zelenograd, Moscow, Russia
*Corresponding Author: Zhandos Tolepov. Email: zhandos.tolepov@gmail.com

Received: 23 February 2026; Accepted: 09 May 2026; Published: 02 June 2026

ABSTRACT: Amorphous selenium (a-Se) thin films were deposited by vacuum thermal evaporation and investigated in planar photoconductive structures to evaluate their optical and photoelectrical properties in the low-field regime. SEM analysis showed continuous film coverage with a thickness of about 250 nm. Raman spectroscopy and X-ray diffraction confirmed the amorphous structure of the as-deposited films and the formation of trigonal crystalline selenium after annealing. Optical analysis based on transmission and reflectance spectra yielded an optical band gap $E_g = 1.96$ eV and an Urbach energy $E_U = 0.083$ eV, indicating localized tail states associated with structural disorder. The planar devices exhibited nearly linear and symmetric dark current-voltage characteristics within $|V| \leq 10$ V, corresponding to an electric field range of 100–1000 V/cm. Under illumination at $\lambda = 633$ nm, the photocurrent showed a sublinear dependence on incident light power density, $I_{\text{photo}} \propto P_{\lambda}^{\gamma}$, with $\gamma = 0.55$. The responsivity increased with the electric field, which indicates more efficient collection of photogenerated carriers at higher bias. Temperature-dependent measurements over the range 303–343 K showed that both the dark current and the current under illumination increase with temperature, whereas the relative photoresponse decreases because the dark current increases more rapidly. Arrhenius analysis yielded effective activation energies 0.836 eV for the dark current and 0.709 eV for the current under illumination. These results show that the optical disorder parameters and the photoelectrical response are mutually consistent. In weak electric fields, the behavior of planar a-Se films is governed by competition between thermally activated dark conduction and field-assisted collection of photogenerated carriers.

KEYWORDS: Amorphous selenium; thermal evaporation; low-field photoconductivity; planar photodetector; Urbach energy

1 Introduction

Amorphous selenium (a-Se) is a classical photoconductive semiconductor widely used in xerography, xeroradiography, and direct-conversion X-ray detectors because of its high photoconductivity, ability to form large-area uniform thin films, and compatibility with conventional device architectures [1,2]. Thin a-Se films also remain of interest for photosensitive and optoelectronic structures, including devices operating at relatively low voltages [3–5].

In X-ray detectors and related photoconductive structures based on a-Se, high electric fields are typically employed, and charge transport is commonly analyzed within models developed for strong-field conditions; in such studies, typical field values are on the order of 10^5 V/cm and higher [1–3]. At substantially lower

fields, however, carrier collection becomes less efficient, and the measured current and photocurrent become more sensitive to localized states, recombination losses, and structural disorder in the amorphous film [4,5]. Recent investigations of Se-containing thin-film devices also indicate that transport, recombination, and device response remain strongly dependent on material configuration and operating conditions [6].

For amorphous a-Se thin films used in planar structures with a lateral electrode configuration on the same side of the film, the influence of structural disorder should be taken into account, since the photoelectrical characteristics are determined not only by the applied field and device geometry but also by the presence of localized states in the amorphous phase [5]. Since this disorder is reflected in the optical absorption behavior, the analysis of the photoelectrical behavior of such structures can be carried out together with consideration of the optical parameters E_g and E_U [4,5].

Accordingly, the aim of this work is to investigate thermally evaporated a-Se thin films in planar photoconductive structures under low-voltage conditions by means of structural, optical, and photoelectrical characterization, including analysis of current-voltage characteristics, photocurrent, responsivity, and thermally activated transport processes, and to discuss the photoelectrical behavior in relation to the optical parameters E_g and E_U.

2 Materials and Methods

Thin selenium (Se) films were deposited by vacuum thermal evaporation in a high-vacuum chamber at a pressure not exceeding 4.2×10^{-6} Torr. Evaporation was carried out from a quartz crucible loaded with granulated high-purity selenium (5N, ReaChem). The deposition rate was 1 nm/s, and the source-to-substrate distance was 10 cm. Polished silicon and quartz substrates were used for film deposition. Prior to deposition, the substrates were plasma cleaned at 30 W for 15 min to remove surface contaminants. Quartz substrates with pre-patterned aluminum contacts were used for the fabrication of planar photoconductive structures. After deposition, the films were annealed at 100°C for 10 min in flowing argon (50 sccm), with heating and cooling rates of 2°C/min. The film thickness was determined from SEM cross-sections; the average thickness was 250 ± 10 nm.

The structural and phase state of the films was examined by Raman spectroscopy and X-ray diffraction (XRD). Raman spectra were recorded at room temperature using an NT-MDT Solver Spectrum system with 633 nm laser excitation; the laser power on the sample was 0.5 mW. XRD measurements were carried out using a Rigaku MiniFlex 600 diffractometer with Cu Kα radiation $(\lambda = 1.5406$ Å$)$. Diffraction patterns were collected over the 2θ range of 5–90°. Data processing, phase identification, and evaluation of lattice parameters were performed using the diffractometer software.

Transmission $T(\lambda)$ and reflectance $R(\lambda)$ spectra of the amorphous selenium (a-Se) films were measured in the wavelength range $\lambda = 200$–1500 nm using an Agilent Cary 5000 spectrophotometer at room temperature. An uncoated quartz substrate served as the reference. The absorption coefficient $\alpha(h\nu)$ [cm^{-1}] was calculated from the measured $T(\lambda)$ and $R(\lambda)$, taking into account the film thickness d [nm], using a homogeneous absorbing film model with reflection losses:

$$\alpha(h\nu) = \frac{1}{d} \ln\left(\frac{(1 - R(h\nu))^2}{T(h\nu)} \right) \quad (1)$$

In Eq. (1), the film thickness d was converted from nm to cm to ensure dimensional consistency. In the spectral region used for band-edge analysis, the interference fringes were not considered. The absorption coefficient α was evaluated and analyzed only in the strong-absorption region near the absorption edge, where the influence of thin-film interference on $T(\lambda)$ is minimized.

The optical band gap E_g [eV] was determined using the Tauc method by linear fitting in the $(\alpha h\nu)^{1/2} - h\nu$ coordinates and extrapolation of the linear region to the energy axis. The Urbach energy E_U [eV] was evaluated from the exponential absorption edge according to the Urbach rule:

$$\alpha(h\nu) = \alpha_0 \exp\left(\frac{h\nu}{E_U}\right) \tag{2}$$

For E_U determination, the linear region of the lnα vs. hν dependence was selected and fitted linearly, and E_U was taken as the inverse slope of this region.

Current-voltage (I-V) characteristics were measured at room temperature using a Tektronix PWS2326 voltage source and a Keithley 6485 picoammeter, both in the dark and under illumination. The photodetector had a planar geometry on a quartz substrate, with aluminum electrodes patterned through a mask. The interelectrode gap was $L = 100$ μm, and the electrode width was 2 mm. The effective active area used for responsivity calculations was defined as the interelectrode channel area, $S = L \cdot W = 2 \times 10^{-3}$ cm^2.

Photoelectrical measurements were performed under illumination with a 633 nm LED (central wavelength λ_c = 633 nm, FWHM $\Delta\lambda$ = 21 nm, specified by the manufacturer). The power density of light P_λ [mW/cm^2] on the sample was set to 0.31, 1.56 and 4.26 mW/cm^2. The photocurrent was defined as the difference between the current under illumination (I_{light}) and the dark current (I_{dark}):

$$I_{\text{photo}} = I_{\text{light}} - I_{\text{dark}} \tag{3}$$

The electric field E [V/cm] was estimated as $E = V/\text{L}$. The dependence I_{photo} (P) was approximated by the power law $I_{\text{photo}} \propto P_\lambda^\gamma$; the exponent γ was extracted by linear fitting of the experimental data in double-logarithmic coordinates. The I_{photo} (P) measurements were carried out at a fixed bias of 10 V.

The responsivity R [A/W] was calculated as the ratio of the photocurrent I_{photo} [A] to the incident optical power P_{inc} [W]:

$$R = \frac{I_{\text{photo}}}{P_{\text{inc}}} \tag{4}$$

where P_{inc} is the optical power incident on the active area. Since the illumination level was specified as the light power density P_λ, P_{inc} was determined as $P_{\text{inc}} = P_\lambda S$, where S is the active area of the photodetector.

3 Results and Discussion

SEM analysis showed that the as-deposited Se film formed a continuous layer without visible cracks or large agglomerates in the examined area (Fig. 1a). The cross-sectional SEM image showed that the film thickness was about 250 nm (Fig. 1b). These observations indicate that vacuum thermal evaporation under the selected conditions provides a morphologically uniform film suitable for further structural, optical, and photoelectrical characterization.

The structural and phase state of the Se films was investigated by Raman spectroscopy and X-ray diffraction. As shown in Fig. 1c, the Raman spectrum of the as-deposited film is characterized by a broad band with a maximum near 252 cm^{-1}, which is typical of a disordered atomic arrangement associated with distorted selenium chains and rings. In addition, a weak feature is observed near 234 cm^{-1}, which may indicate the presence of a minor fraction of the trigonal phase. After annealing, the broad amorphous band disappears, whereas the peak near 234 cm^{-1} becomes more intense and narrower, which is consistent with

the formation of trigonal crystalline selenium [7,8]. Fig. 1d schematically shows the atomic arrangements in the amorphous and trigonal crystalline films.

To further confirm the phase state of the Se films before and after annealing, X-ray diffraction analysis was performed. As shown in Fig. 1e, the as-deposited film exhibits a broad diffuse halo characteristic of the amorphous state, indicating the absence of long-range order. In contrast, the annealed film shows distinct diffraction peaks assigned to trigonal selenium (space group P3121). The refined lattice parameters are $a = 4.359$ Å, $b = 4.359$ Å, and $c = 4.951$ Å, which are in good agreement with the reported crystal structure of trigonal selenium [9].

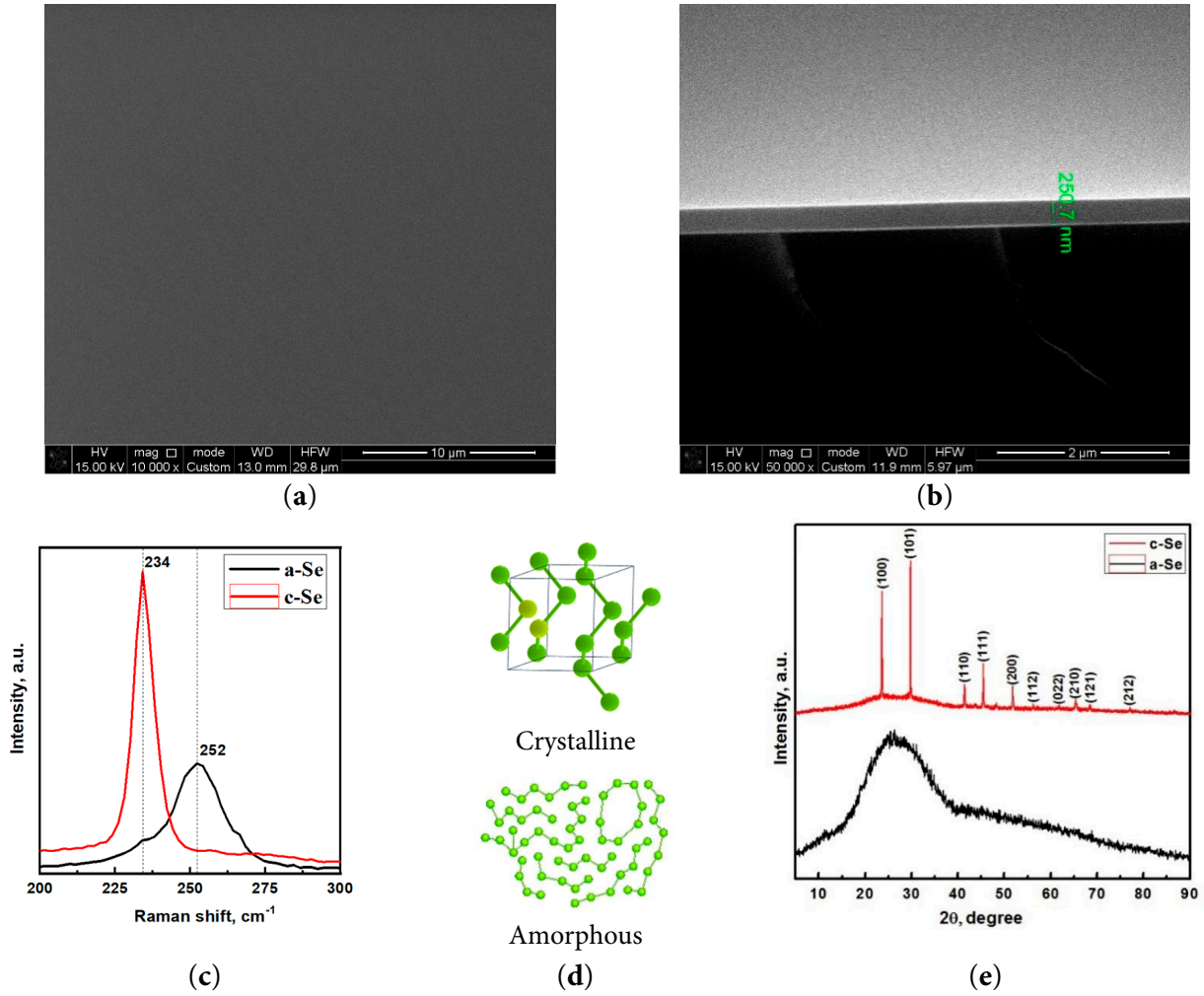

Figure 1: (**a**) Surface SEM image of the as-deposited Se film; (**b**) cross-sectional SEM image showing the film thickness; (**c**) Raman spectra of amorphous (a-Se) and crystallized (c-Se) selenium films; (**d**) schematic models of the amorphous network and trigonal Se lattice; (**e**) XRD patterns of amorphous and crystallized Se films.

Fig. 2a,b shows the transmission and reflectance spectra of the amorphous selenium (a-Se) film. In the short-wavelength region, the transmittance remains low and increases toward longer wavelengths, whereas the reflectance exhibits a weaker nonmonotonic spectral dependence. These spectra were used to calculate the absorption coefficient $\alpha(h\nu)$, which served as the basis for the subsequent determination of the optical band gap and the Urbach energy [10].

Fig. 2c shows the Tauc plot in the $(\alpha h\nu)^{1/2}$ vs. $h\nu$ coordinates. A linear region is observed near the absorption edge, which allows the optical band gap E_g to be determined by extrapolating the linear fit to the photon-energy axis [11–13]. The linear fit was performed in the photon-energy range of 2.09–2.25 eV. The resulting value was $E_g = 1.96 \pm 0.01$ eV [4,5].

Fig. 2d presents the $\ln \alpha$ versus $h\nu$ dependence used for the Urbach analysis. A linear segment corresponding to the exponential increase of α is clearly distinguished. The Urbach energy E_U was determined according to Eq. (2) as the inverse slope of the linear fit in the photon-energy range of 2.05–2.15 eV. The resulting value was $E_U = 0.083 \pm 0.002$ eV [4,5,12,14].

The Urbach energy E_U reflects the exponential tail of localized states near the band edges and local potential fluctuations caused by structural disorder in the amorphous network. Thus, the parameters E_g and E_U provide a consistent description of the absorption edge in a-Se: E_g defines the energetic position of the interband absorption edge, whereas E_U characterizes the degree of exponential broadening in the sub-gap absorption region typical of amorphous semiconductors [12,14]. The obtained values, $E_g = 1.96$ eV and $E_U = 0.083$ eV, lie within the range reported for amorphous selenium films and are therefore consistent with the expected optical behavior of disordered a-Se [4,5].

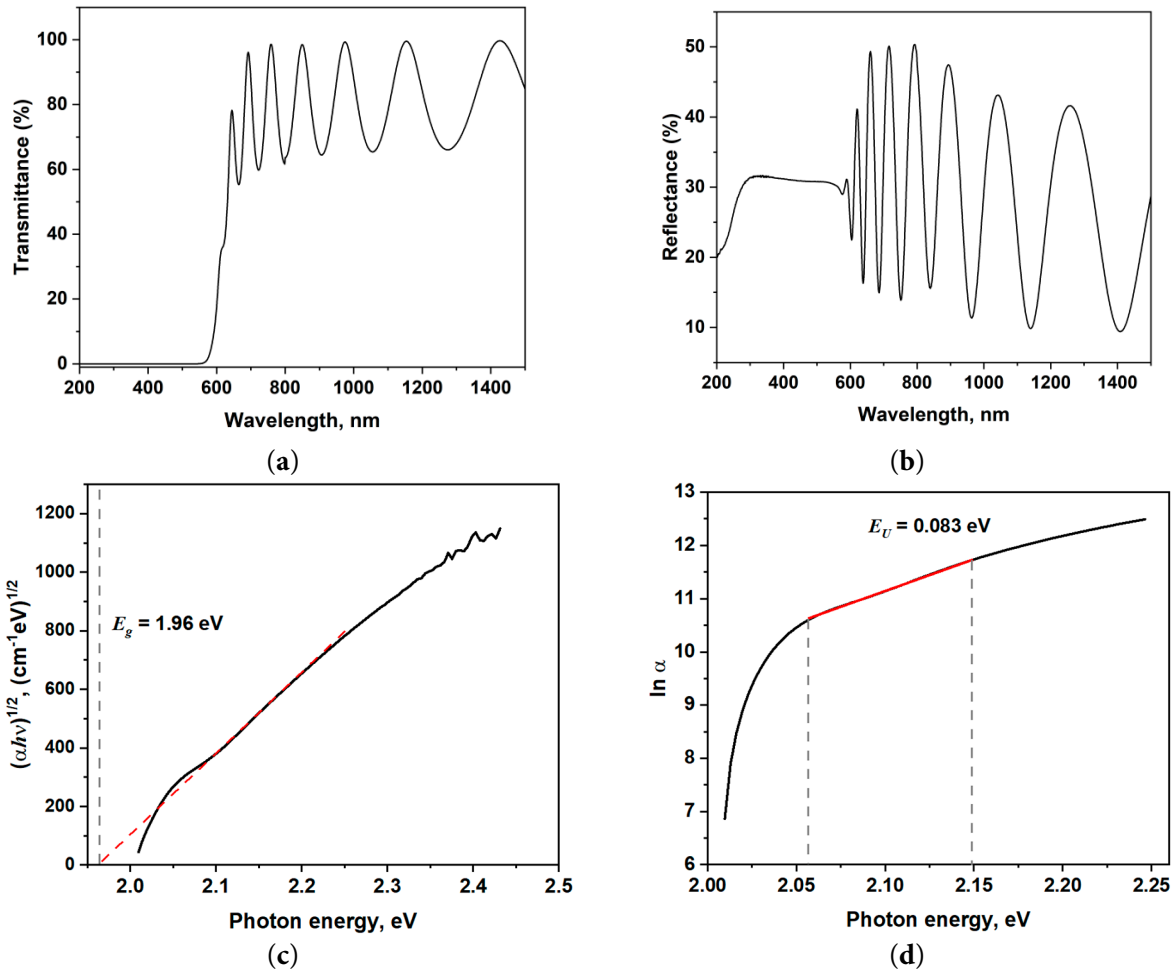

Figure 2: Optical characterization of the amorphous selenium (a-Se) film: (**a**) transmission spectrum; (**b**) reflectance spectrum; (**c**) Tauc plot used for determination of the optical band gap E_g; (**d**) Urbach plot ($\ln \alpha$ vs. $h\nu$) used for determination of the Urbach energy E_U.

Fig. 3a,b shows the schematic of the planar a-Se photodetector and the optical image of the fabricated structure. The device has a lateral geometry with aluminum electrodes located on the same side of the quartz substrate, and the interelectrode gap is 100 μm. This configuration corresponds to the planar photoconductive structure used to investigate the photoelectrical properties of the amorphous selenium film under low-voltage conditions.

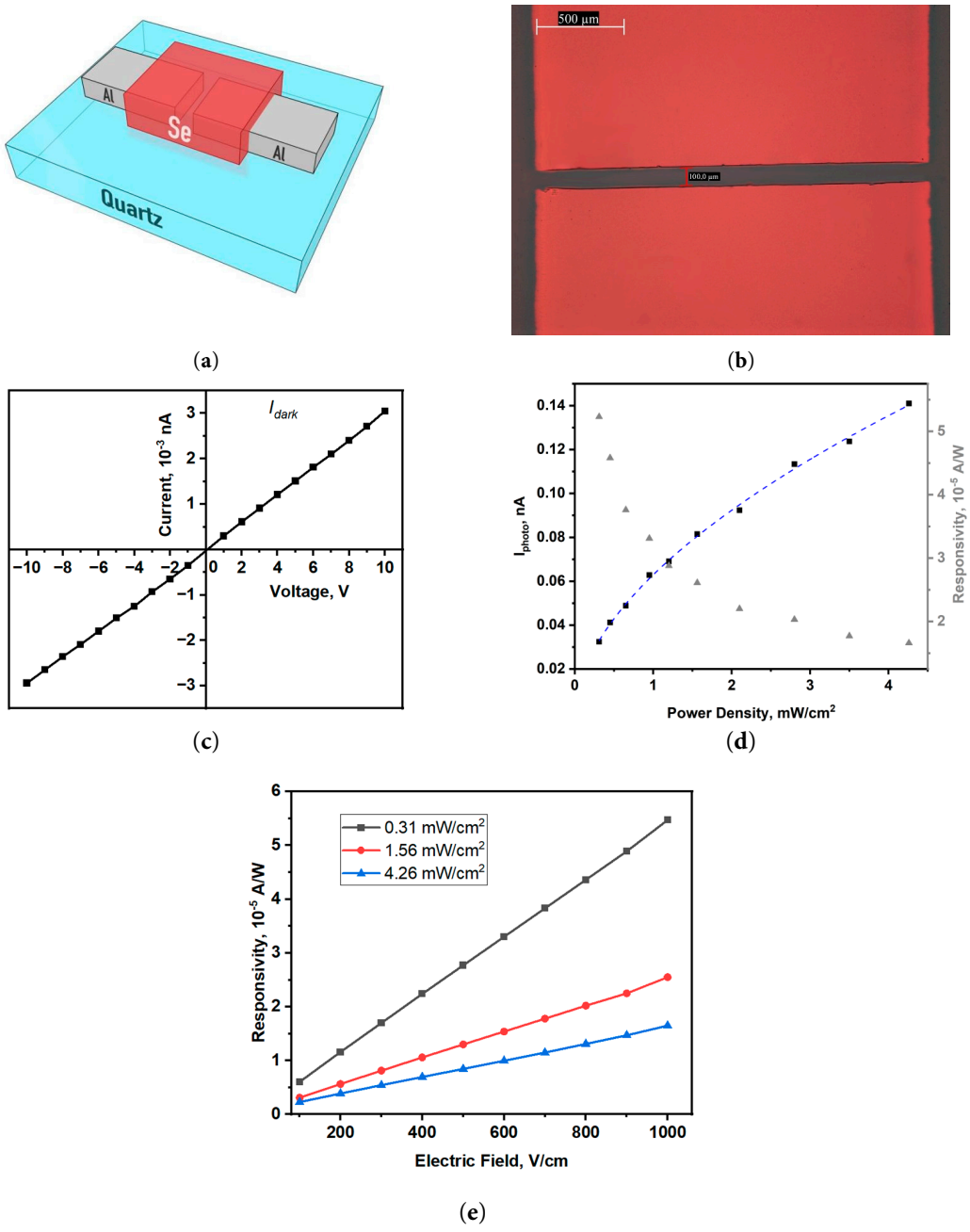

Figure 3: (**a**) Schematic of the planar a-Se photodetector with Al electrodes on a quartz substrate; (**b**) optical image of the planar structure; (**c**) dark current-voltage (I-V) characteristic measured at room temperature; (**d**) photocurrent I_{photo} as a function of incident light power density P_λ at V = 10 "V" (left axis) and responsivity R as a function of P_λ (right axis); (**e**) responsivity R as a function of electric field E at λ = 633 "nm" for different illumination levels.

The dark current-voltage characteristic presented in Fig. 3c is nearly linear and symmetric within the investigated voltage range. This indicates the absence of pronounced rectifying asymmetry in the contact configuration used and suggests that, within this bias range, the transport can be considered in terms of a quasi-linear response of the structure. At the same time, the absolute values of the dark current remain low, which is important for resolving the photoinduced response at low bias voltages.

Fig. 3d shows the dependence of the photocurrent on the incident light power density at $\lambda = 633$ nm and $V = 10$ V. With increasing light power density, the photocurrent increases; however, the dependence is sublinear. Fitting the experimental data with the power law $I_{\text{photo}} \propto P_{\lambda}^{\gamma}$ yields $\gamma < 1$, indicating a deviation from an ideal linear photoresponse. Such behavior is commonly associated with the influence of localized states, carrier trapping, and recombination losses, whose contribution becomes significant in amorphous photoconductive materials at low electric fields [5,12].

The dependences of responsivity on the electric field for different illumination levels are shown in Fig. 3e. In all cases, the responsivity increases with increasing field, which is naturally related to more efficient collection of photogenerated carriers as the field strength in the interelectrode channel increases. At the same time, the responsivity is lower at higher light power densities, which is consistent with the observed sublinear I_{photo} (P_{λ}) dependence. Taken together, these results show that planar structures based on thermally evaporated a-Se exhibit a stable photoelectric response at low bias voltages, while its magnitude is governed by the combined influence of the electric field and the incident light intensity.

To further clarify the low-field transport regime, temperature-dependent measurements of the dark current and the current under illumination were performed in the range 303–343 K at a fixed bias of 5 V. As shown in Fig. 4a, both the dark current I_{dark} and the current under illumination I_{light} increase with increasing temperature. However, the dark current increases much faster than the photoinduced current increment, defined as $I_{photo} = I_{light} - I_{dark}$, which leads to a monotonic decrease in the ratio I_{photo}/I_{dark}, as shown in Fig. 4b. This behavior indicates that, in the studied low-field regime, the useful photoresponse becomes less pronounced with increasing temperature because of the faster growth of the thermally activated dark current.

The observed behavior is qualitatively consistent with low-field transport in disordered amorphous selenium involving localized tail states. As the temperature increases, thermally activated release of carriers from localized states enhances the background dark conduction, in agreement with previous reports that the dark current in a-Se thin films is thermally activated above room temperature [15]. At the same time, the photoinduced current increment increases much more weakly, because trapping and recombination losses remain significant. As a result, the photoresponse contrast decreases with temperature, which is consistent with trap-assisted transport under weak electric fields.

For a more quantitative interpretation, the experimental data were analyzed in Arrhenius coordinates. Fig. 4c shows the dependences of $\ln I$ on $1000/\text{T}$ for the dark current and the current under illumination. Both dependences are satisfactorily approximated by straight lines, indicating thermally activated conduction in the studied temperature interval. The effective activation energies determined from the slopes of these dependences were 0.836 eV for the dark current and 0.709 eV for the current under illumination. The thermally activated character of the dark current is consistent with previous observations in amorphous selenium thin films, where activation energies close to 1 eV were reported above room temperature [15]. The stronger temperature dependence of the dark current shows that, in the low-field regime, the thermally activated background conduction increases faster than the photoinduced current increment.

For the estimation of transport parameters, literature data typical of undoped amorphous selenium were used [1,2]. According to published data, the typical hole mobility is $\mu_h \approx 0.13$–0.14 cm^2 V^{-1} s^{-1},

whereas the typical $\mu\tau_h$ range is of the order of 10^{-6}–10^{-5} cm^2/V. On this basis, the carrier drift length was estimated using the relation $l_d = \mu\tau E$ in the investigated electric-field range. The obtained values are of the order of 1–10 μm at 100 V/cm and 10–100 μm at 1000 V/cm. Since the interelectrode gap in the planar structure under study is 100 μm, these estimates indicate incomplete carrier collection at low fields and improved drift collection with increasing field.

It should be noted that the Urbach energy E_U, the sublinearity parameter γ, and the observed temperature dependences of the current are not directly equivalent quantities; however, they are qualitatively consistent with the general picture of low-field transport in disordered a-Se involving localized tail states and trapping processes. The nonzero value of E_U reflects the presence of a tail of localized states near the band edges, whereas $\gamma < 1$ and the pronounced thermal activation of the dark current indicate the significant role of trapping and recombination losses in the formation of the photoresponse.

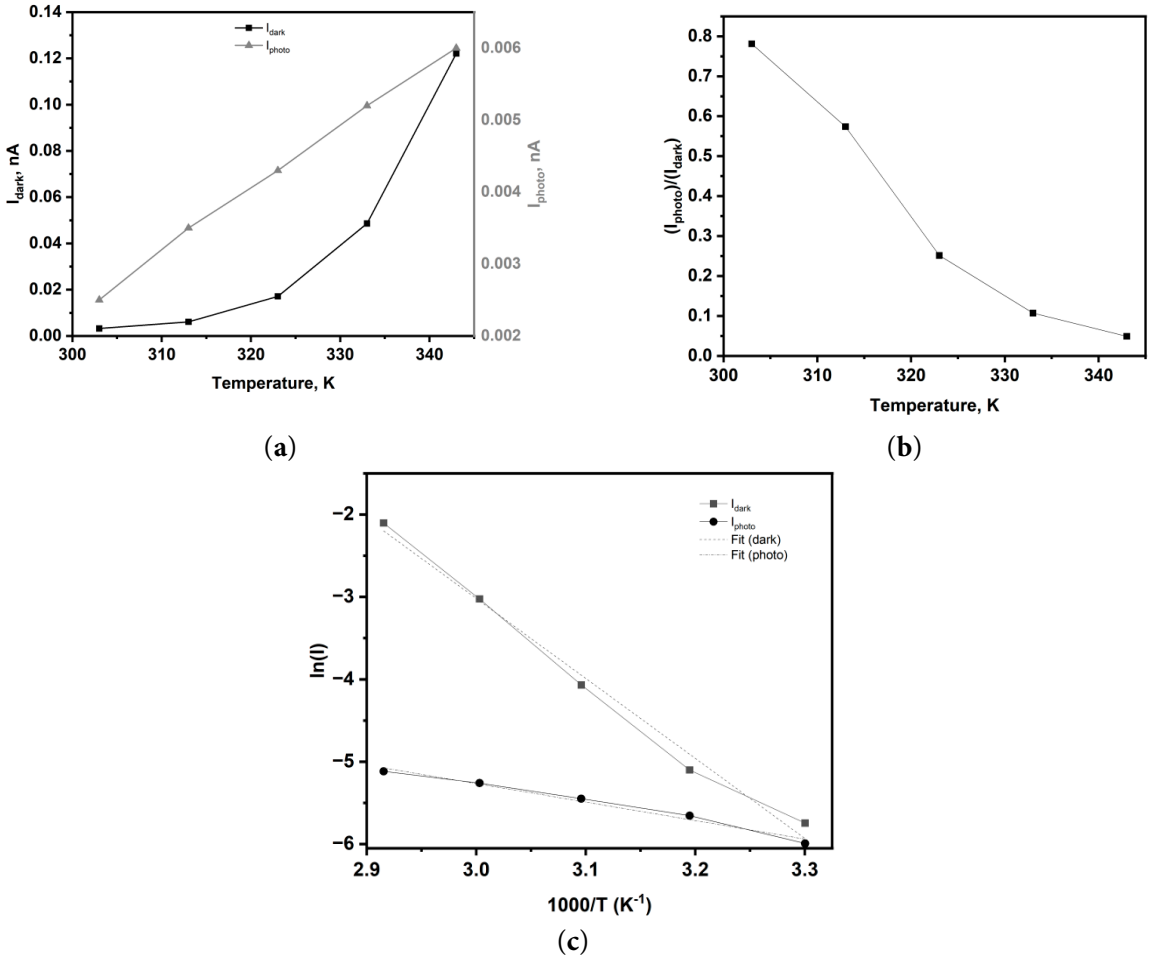

Figure 4: Temperature-dependent electrical characteristics of the planar a-Se structure measured at a fixed bias of 10 V; (**a**) temperature dependences of the dark current I_{dark} and the photoinduced current increment I_{ph}; (**b**) temperature dependence of the ratio I_{ph}/I_{dark}; (**c**) Arrhenius plots, ln(I) versus 1000/T, for the dark current and the current under illumination.

Thus, the estimation of transport parameters together with the temperature-dependent measurements shows that, in the studied range of weak electric fields, the photoresponse of planar a-Se films is determined

by the competition between the thermally activated increase in dark conduction and the limited collection of photogenerated carriers. At low fields, the drift length remains smaller than the interelectrode gap, which leads to incomplete carrier collection, whereas increasing the field improves drift collection, in agreement with the experimentally observed increase in responsivity.

4 Conclusion

In this work, planar photodetectors based on thermally evaporated amorphous selenium (a-Se) films with Al electrodes were fabricated and investigated using optical and temperature-dependent electrical measurements. Optical absorption analysis yielded an optical band gap of $E_g = 1.96$ eV and an Urbach energy of $E_U = 0.083$ eV. These values are consistent with the disordered electronic structure of amorphous selenium and indicate the presence of localized tail states near the band edges.

The electrical measurements showed that, in the studied weak-field range, the photoresponse is governed by the competition between thermally activated dark conduction and limited collection of photogenerated carriers. Literature-based estimates of the transport parameters showed that, at low electric fields, the carrier drift length, $L_d = \mu\tau E$, remains smaller than the interelectrode gap. This condition leads to incomplete carrier collection and therefore reduces the photoresponse. Increasing the electric field improves carrier collection and increases responsivity, in agreement with the experimental results.

Temperature-dependent measurements further showed that increasing temperature enhances the dark current through thermally activated transport. As a result, the relative photoresponse decreases even though a measurable photocurrent remains present. Therefore, the performance of planar a-Se photodetectors in weak electric fields is determined by the balance between field-assisted carrier collection and temperature-induced growth of dark conduction.

Overall, the results clarify the mechanisms limiting the performance of planar a-Se photodetectors under low-field conditions. Further improvement requires increasing the effective electric field, reducing the carrier transit distance, or optimizing the device geometry to enhance carrier collection before recombination and trapping losses become dominant.

Acknowledgement: The authors would like to thank Guseinov N. R., Nemkayeva R. R., and Orynbai B. for their valuable advice and support.

Funding Statement: The authors received no specific funding for this study.

Author Contributions: The authors confirm contribution to the paper as follows: conceptualization, Zhandos Tolepov and Oleg Prikhodko; film deposition and sample preparation, Guzal Ismailova; investigation and device design, Zhadyra Toreniyaz and Nurkadam Tolep; XRD analysis, Zhasulan Nakysbekov; Raman analysis, Tilek Kuanyshbekov; optical measurements, Dmitry Terekhov. All authors reviewed and approved the final version of the manuscript.

Availability of Data and Materials: The data supporting the findings of this study are available from the corresponding author upon reasonable request.

Ethics Approval: Not applicable.

Conflicts of Interest: The authors declare no conflicts of interest.

References

1. Kasap SO, Rowlands JA. Review: X-ray photoconductors and stabilized a-Se for direct conversion digital flat-panel X-ray image detectors. J Mater Sci Mater Electron. 2000;11:179–98. [CrossRef].

2. Huang H, Abbaszadeh S. Recent developments of amorphous selenium-based X-ray detectors: a review. IEEE Sens J. 2020;20(4):1694–704. [CrossRef].
3. Hellier K, Swaby A, Ott J, Abbaszadeh S. Performance evaluation of an amorphous selenium photodetector at high fields for application integration. IEEE Sens J. 2023;23(12):12759–66. [CrossRef].
4. Al-Ani SKJ, Al-Delaimi MN, Al-Hamdani AH, Jawher HM. Optical and electrical properties of pure and doped amorphous thin selenium films. Int J Electron. 1990;69(1):87–95. [CrossRef].
5. Tanaka K, Gotoh T. Gap states in amorphous selenium: what are the atomic structures? Phys Status Solidi B. 2025;262(4):2400458. [CrossRef].
6. Tian J, Zhang Q, Wu L, Hao X, Zeng G, Wang W, et al. Impact of window layers on selenium distribution and photovoltaic performance in $CdSe_xTe_{1-x}$/CdTe solar cells. Chalcogenide Lett. 2026;23(1):2. [CrossRef].
7. Hesabizadeh T, Subedi R, Webster TJ, Guisbiers G. Selenium nanoparticles: effect of autoclave treatment on size, shape, phase and antimicrobial properties. Chalcogenide Lett. 2024;21(11):847–54. [CrossRef].
8. Poborchii VV, Kolobov AV, Tanaka K. An *in situ* Raman study of polarization-dependent photocrystallization in amorphous selenium films. Appl Phys Lett. 1998;72(10):1167–9. [CrossRef].
9. Cherin P, Unger P. The crystal structure of trigonal selenium. Inorg Chem. 1967;6(8):1589–91. [CrossRef].
10. Sharma I, Sharma P, Hassanien AS. Optical properties and optoelectrical parameters of the quaternary chalcogenide amorphous $Ge_{15}Sn_xS_{35-x}Te_{50}$ films. J Non-Cryst Solids. 2022;590:121686. [CrossRef].
11. Tauc J, Grigorovici R, Vancu A. Optical properties and electronic structure of amorphous germanium. Phys Status Solidi B. 1966;15(2):627–37. [CrossRef].
12. Davis EA, Mott NF. Conduction in non-crystalline systems V. Conductivity, optical absorption and photoconductivity in amorphous semiconductors. Philos Mag. 1970;22(179):903–22. [CrossRef].
13. Özmenteş R, Hassanien AS. Characterizations and optical discussions of thermally evaporated titanium dioxide thin films. J Opt. 2025;54(3):1322–40. [CrossRef].
14. Urbach F. The long-wavelength edge of photographic sensitivity and of the electronic absorption of solids. Phys Rev. 1953;92(5):1324. [CrossRef].
15. Qamhieh N, Willekens J, Brinza M, Adriaenssens GJ. Anomalous DC dark conductivity behaviour in a-Se films. J Phys Condens Matter. 2003;15(41):L631–7. [CrossRef].